The editorial pdf is reachable at

https://doi.org/10.1016/j.bbamem.2021.183667

Calixarene-based artificial ionophores for chloride transport across natural liposomal bilayer: synthesis, structure-function relationships, and computational study

Serena Pilato[a], Massimiliano Aschi[b], Margherita Bazzoni[c], Federica Cester Bonati[c], Gianpiero Cera[c], Samanta Moffa[a], Valentino Canale[a], Michele Ciulla[a], Andrea Secchi[c], Arturo Arduini[c], Antonella Fontana[a] and Gabriella Siani[a*]

[a]Dipartimento di Farmacia, Università "G. d'Annunzio", Chieti, Italy; [b]Dipartimento di Scienze Fisiche e Chimiche, Università degli Studi dell'Aquila, Coppito, Italy; [c]Dipartimento di Scienze Chimiche, della Vita e della Sostenibilità Ambientale, Università di Parma, Parco Area delle Scienze 17/A, I-43124 Parma, Italy.

*corresponding author: e-mail: siani@unich.it.

An amphiphilic calix[6]arene, alone or complexed with an axle to form a pseudo-rotaxane, has been embedded into liposomes prepared from 1-palmitoyl-2-oleoyl-sn-glycero-3-phosphocholine (POPC) and the permeability of the membrane-doped liposomes towards Cl^- ions has been evaluated by using lucigenin as the fluorescent probe. The pseudo-rotaxane promotes transmembrane transport of Cl^- ions more than calix[6]arene does. Surprisingly, the quenching of lucigenin was very fast for liposomes doped with the positively charged axle alone. Molecular dynamics (MD) simulations and quantum-chemical calculations were also carried out for providing a semi-quantitative support to the experimental results.

Keywords: liposomes; calixarenes; pseudo-rotaxanes; ion channel; anion-π interactions

1. Introduction

Transport of ions across the membrane is a fundamental process for living cells (1). Indeed, defects in the transmembrane ion transport mechanism can cause serious diseases and even lead to death (2, 3). This is the case of cystic fibrosis, caused by a mutation in the cystic fibrosis transmembrane conductance regulator (CFTR) protein which is involved in the transport of chloride ions (4).

While small, neutral, and hydrophobic molecules can pass the semi-permeable bilayer, ions cannot diffuse across the membrane and their transport must be assisted by carrier proteins or supramolecular channels made of protein subunits which self-assemble to form a pore across the bilayer, through which the ions can move in single lines.

Therefore, much of the research has been recently directed towards the engineering of artificial ion channels to discover new therapeutic strategies for the channelopathies caused by a dysregulated ion transport.

A number of synthetic channels has been designed for the transmembrane transport of anions and most of them have been obtained by self-assembly of simple building units (5). For example, a synthetic chloride membrane transporter based on the association of two molecules of a heptapeptide has been developed and characterized by Gokel (6). Recently, Zeng et al. have described peptidic rod-like structures which oligomerize to form pores with high anion-transport activity (7). Self-assembled transmembrane anion channels have also been obtained by small-molecule fumaramides (8).

Among the systems potentially useful as synthetic ionophores, calixarenes have recently gained considerable attention due to their fascinating properties. Indeed, the ability of calixarenes to form complexes with a large variety of compounds, both ionic and neutral species, has been well demonstrated so that their internal cavity can act as a

biomimetic filter. The most interesting aspect of the chemistry of calixarenes is that their properties can be easily tuned by introducing suitable functional groups on their upper and lower rim to optimize their use in a variety of applications, from molecular recognition (9) to drug carriers (10). Proper modifications in the basic structure of calixarenes have led to selective binding for anions (11), cations (12), and neutral species (13). Moreover, amphiphilic calixarenes can be prepared by introducing long alkyl chains which allow them to be inserted into lipid bilayers (14, 15).

Although most of the studies on the ability of calixarenes to promote transmembrane transport were initially focused on the transport of cations (16-19), in particular Na^+ and K^+, interest has recently grown in their potential Cl^- channel-like behaviour. Studies have been reported on the ability of properly functionalized calix[4]arenes to form channels that show H^+/Cl^- symport activity (20-22). Lipophilic calix[4]arene amides in their cone conformation have been successfully used as mobile carriers to shuttle Cl^- ions across lipid membranes (23). More recently, the formation of pores by hydrophobic ureido-calix[6]arene, which can promote transmembrane chloride transport across the lipid bilayer, has been reported (24).

Anion recognition and transport across membranes was generally achieved by electrostatic attraction and hydrogen bonding between anion and ionophore. Indeed, most synthetic anion transporters contain hydrogen bonding donors such as pyrrole (25-27), amide or urea groups (21, 22, 28) or positively charged groups which can electrostatically attract the anions (20, 29, 30).

Davis et al. have demonstrated that the hydrogen bond donor secondary amide group is necessary but non-sufficient to facilitate anion transport across bilayers as the compound's conformation and its self-association properties are important for this function (31). Moreover, beside the classical hydrogen bonding, many studies have

demonstrated that the unorthodox non-covalent interaction between anions and electron-deficient π systems could play a primary role to lower the energy barrier for selective anion transmembrane transport (32-35). Anion-π interactions have been extensively studied computationally (36-38) and, recently, they have aroused considerable attention in the field of supramolecular chemistry. While the interaction between electron-rich aromatic rings and anions is thermodynamically disfavoured, the occurrence of non-covalent binding mode between an anion and an electron-deficient aromatic ring has been demonstrated (39-41). A number of receptors able to bind anions through electron-deficient arenes have been designed (42) and often additional attractive forces such as hydrogen bonding have been used to help the anion recognition (43). Based on this new type of non-covalent interaction, many artificial ion channel and carriers have been developed for an efficient anion transfer across lipid bilayers (34,35,44,45).

Indeed, defining the relationship between the structure of the synthetic ionophore and its ability to facilitate the transport of anions appears to be of fundamental importance for understanding the complex mechanism of the process and this knowledge could allow designing the best system for the most efficient ion transport across membranes. Calixarenes are ideally suited to this task as they can be easily modified by adding proper functional groups as a part of the scaffold.

Besides the direct ion/ionophore interaction, in some cases, also the ionophore/membrane interactions can explain the transmembrane passage of the ions. Recently, D'Errico et al. have explored the interactions of some artificial ionophores, i.e., PEGylated cyclic oligosaccharides (46) and guanosine-based amphiphiles (47) with DOPC:DOPG phospholipid membranes by DLS, electron spin resonance (ESR) and neutron reflectivity (NR) measurements. The Authors concluded that the ion transport across the membrane occurs through a non-specific mechanism related to the

perturbation of the bilayer induced by the ionophore insertion which leads to disorder of the lipid acyl chains and/or variation of the local polarity across the membrane.

In this paper, we report on the Cl^- transport activity of a calix[6]arene designed for obtaining an amphiphilic molecule in which long hydrophobic tails on the lower rim allow it to be inserted into lipid bilayers. Ureido groups have been introduced on the upper rim as hydrogen bonding donors to bind chloride ions and enable their transport as well as to match the phospholipid heads. Pyridine moieties were introduced on ureidic nitrogen atoms to provide anion-π interactions. The structure of calix[6]arene **1** is reported in Figure 1. Finally, the pseudo-rotaxane **2** of Figure 1 has been obtained by complexing calix[6]arene with the axle **3**, a C12- alkyl chain bearing a styryl pyridinium group on one end and a viologen group on the other end.

The obtained results have been compared with those achieved in a previous study performed on a tris-(*N*-phenylureido)calix[6]arene (24).

Moreover, the changes in lipid bilayer properties, i.e., microviscosity, liposome dimension, surface charge and stability, induced by the incorporation of the guests, have been investigated.

Molecular dynamics (MD) simulations and quantum-chemical calculations were also carried out for providing a semi-quantitative support to our experimental results.

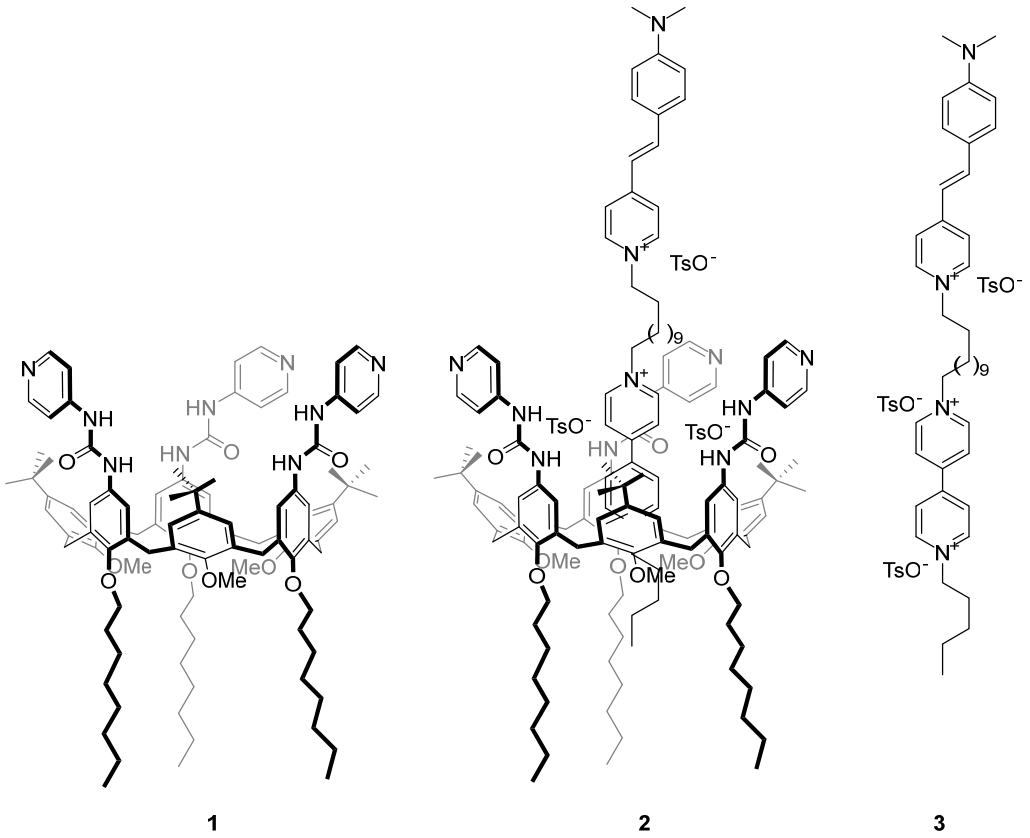

Figure 1. Structures of the calix[6]arene **1**, the pseudo-rotaxane **2** and the axle **3** used as guest in the POPC liposomes.

2. Experimental section

2.1 Materials

1-palmitoyl-2-oleoyl-*sn*-glycero-3-phosphocholine (POPC) was purchased from Avanti Polar Lipids (Alabaster, AL). The fluorescent probes 5(6)-carboxyfluorescein (CF), pyrene and lucigenin, tetrabutylammonium chloride, $CHCl_3$, CH_2Cl_2, CH_3OH, CH_3CH_2OH, $CDCl_3$, Triton X-100, Sephadex G-25 and the salts used for the preparation of buffers were purchased from Sigma Aldrich and used without further purification.

Reactions were monitored by TLC using 0.25 mm Merck silica gel plates (60 F254). Solvents were dried using an Inert Pure Solv Micro Apparatus and stored over

molecular sieves. All other reagents were of reagent grade quality, obtained from Sigma Aldrich, and used without further purification. “Brine” refers to a saturated aqueous solution of NaCl. Unless otherwise specified, solutions of common inorganic salts used in workups are aqueous solutions. Triamino calix[6]arene (**4**), (48) (*E*)-*N*,*N*-dimethyl-4-(2-(pyridin-4-yl)vinyl)aniline (**5**), (49) and 1-pentyl-[4,4'-bipyridin]-1-ium tosylate (**8**) (50) were synthesized according to published procedures.

2.2 Instruments

Fluorimetric measurements have been carried out on Jasco FP-6200 or Jasco FP-6500 spectrofluorimeters. UV-Vis absorption measurements have been performed on a Jasco V-550UV/Vis spectrophotometer.

The size and ζ potential values of the pure and loaded POPC liposomes were measured by using a 90Plus/BI-MAS ZetaPlus multiangle particle size analyzer (Brookhaven Instruments Corp., Holtsville, NY).

Automated flash column chromatography purifications were done using a Teledyne Isco apparatus with prepacked silica gel columns. m/z of compounds were assessed in the ESI mode using a Thermo LTQ ORBITRAP XL (HR-MS) and a Waters Acquity Ultra Performance LC instruments. ^{1}H and ^{13}C NMR spectra were recorded on a Bruker Avance III spectrometer operating at 400 and 100 MHz, respectively. Chemical shifts (δ) are reported in parts per million (ppm) using the residual solvent signal as an internal reference (7.26 ppm for $CHCl_3$ and 3.34 ppm for CD_2HOH).

For titration experiments, ^{1}H-NMR spectra were recorded on a Bruker Avance 300 spectrometer with ^{1}H at 300.060 MHz. Proton chemical shifts were referenced to the TMS internal standard. Chemical shifts are reported in parts per million (ppm, δ units).

2.3 Synthesis

Tris-(pyridin-4-yl)ureido calix[6]arene (1) In a 250 ml round bottom flask kept under nitrogen atmosphere, to a solution of triphosgene (0.092 g, 0.31 mmol) in 100 ml of dry toluene, a solution of trioctyl-triamino calix[6]arene **4** (0.35 g, 0.28 mmol) and trietylamine (0.09 g, 0.92 mmol) in 50 ml of dry toluene was dropwise added. The resulting reaction mixture was stirred at 80 °C for 2 hours, then cooled to room temperature and 4-aminopyridine (0.13 g, 1.4 mmol) was added. After 3 hours of stirring at 80°C, the solvent was removed under vacuum, and the residue taken up with 100 mL of dichloromethane. The resulting organic solution was washed thrice with distilled water, dried over anhydrous sodium sulphate, and evaporated to dryness. Purification of the residue by column chromatography (eluent dichloromethane / methanol = 8 / 2) afforded 0.24 g (55%) of **1** as a yellow solid. M.p. 206-208 °C; ^{1}H NMR ($CDCl_3$, 400 MHz) δ = 8.2, 8.0, 7.3, 7.1, and 6.6 (5 br. s, 24H); 4.5, 3.9, 3.5, and 2.8 (4 br. s, 27H); 1.9, 1.6, 1.5-1.2, and 0.9 (br. s, br. s, m, br. t, 76H); ^{13}C NMR ($CDCl_3$, 100 MHz) δ = 127.9 (br. s, CH), 112.7 (br. s, CH), 73.5 (CH_2), 34.3 (br. s, C_q), 31.9 (CH_2), 31.6 (CH_3), 30.6, 29.6, 29.3, 26.4, 22.7 (5 CH_2), 14.1 (CH_3); HR-MS (ESI, Orbitrap LQ) calculated for $C_{99}H_{130}N_9O_9$ [M+H] m/z (z = 1): 1588.99860 (90%), 1590.00181 (100%), 1591.00496 (58%), 1592.00805 (24%), 1593.01109 (7%); Found: 1588.9996 (90%), 1590.00362 (100%), 1591.00689 (58%), 1592.01036 (22%), 1593.01151 (8%).

Dodecane-1,12-diyl ditosylate (6). In 250 ml round bottom flask, 1,12-dodecanediol (10 g, 0.5 mol), p-toluenesulfonyl chloride (19.5 g, 1.5 mol), triethylamine (15 g, 1.5 mol) and a tip of spatula of 4-(dimethylamino)pyridine (cat.) were solubilised in dry CH_2Cl_2 (100 ml). The reaction mixture was stirred at room temperature for 24 hours and

then quenched by water (100 ml). The separated organic phase was dried over Na_2SO_4 and evaporated to dryness under reduced pressure. The pure product was obtained after precipitation from methanol (85%). M.p. 72-74 °C. ^{1}H NMR (400 MHz, $CDCl_3$) δ = 7.81 (d, 4H, *J* = 8.3 Hz), 7.36 (d, 4H, *J* = 8.0 Hz), 4.04 (t, 4H, *J* = 6.5 Hz,) 2.47 (s, 6H), 1.7 – 1.6 (m, 4H), 1.4 – 1.2 (m, 16H); ^{13}C NMR (100 MHz, $CDCl_3$) δ = 129.8, 127.9, 70.7, 29.4, 29.3, 28.9, 28.8, 25.3; ESI-MS(+) m/z = 533.3 (100), 534.3 (20) $[M+Na]^+$, 549.2 (30), 550.2 (10) $[M+K]^+$.

Synthesis of (*E*)-1-(4-(4-(4-(dimethylamino)styryl)pyridin-1-ium-1-yl)butyl)-1'-pentyl-[4,4'-bipyridine]-1,1'-diium tritosylate (3). In a sealed glass autoclave, a degassed solution of ditosylate **6** (8 g, 15.7 mmol) and pyridine derivative **5** (0.5 g, 2.2 mmol) in dry acetonitrile (5 ml) was refluxed for 12 hours. After cooling to room temperature, the solvent was evaporated to dryness and the solid residue was treated with hot methanol (25 ml). The solid residue of **6** was recovered by filtration, and the solvent evaporated to dryness to afford 0.8 g (65%) of the desired stilbazolium salt **7** as a red solid compound. This compound was used as such to alkylate the pyridyl *N*-pentyl pyridnium tosylate **8**. In detail, a solution of **7** (0.14 g, 0.18 mmol) and **8** (0.086 g, 0.22 mmol) in 10 ml of dry acetonitrile was poured in a small glass autoclave. After two vacuum/nitrogen cycles, the autoclave was sealed, and the solution refluxed for at least 7 days. After this period, the solution was cooled to room temperature. Upon standing at room temperature, a red solid compound precipitated from the reaction solution, which was isolated by suction filtration. After drying under reduced pressure, 0.087 g (41%) of pure **3** were recovered as a red solid compound. M.p. 223-225; ^{1}H NMR (CD_3OD, 400 MHz) δ = 9.24 (dd, 4H, J_1 = 6.8, J_2 = 1.8 Hz), 8.66 (d, 4H, *J* = 6.2 Hz), 8.58 (d, 2H, *J* = 6.6 Hz), 7.97 (d, 2H, *J* = 6.7 Hz), 7.84 (d, 1H, *J* = 15.9 Hz), 7.70 (d, 5H, *J* = 7.9 Hz), 7.62 (d, 2H, *J* = 8.9 Hz), 7.24 (d, 5H. *J* = 7.9 Hz), 7.10 (d, 1H, *J* = 15.9 Hz), 6.80 (d,

2H, *J* = 8.4 Hz), 4.8 – 4.7 (m, 4H), 4.42 (t, 2H, *J* = 7.3 Hz), 3.09 (s, 6H), 2.34 (s, 8H), 2.1 – 2.0 and 2.0 – 1.9 (2m, 6H), 1.5 – 1.3 (3m, 18H), 0.97 (t, 3H, *J* = 6.7 Hz); ^{13}C-DEPTQ NMR (CD_3OD, 100 MHz) δ = 154.9 (C_q), 152.6 (C_q), 149.8 (C_q), 146.6 (br., CH), 143.0 (CH), 142.9 (CH), 142.2 (C_q), 140.3 (C_q), 130.2 (CH), 128.5 (CH), 126.9 (CH), 125.5 (CH), 122.3 (CH), 111.7 (CH), 61.9 (CH_2), 59.8 (CH_2), 38.8 (CH_3), 31.1 (CH_2), 30.8 (CH_2), 29.2 (CH_2), 29.1 (CH_2, 2 res.), 28.8 (CH_2, 2 res.), 27.9 (CH_2), 25.9 (CH_2), 25.8 (CH_2), 21.8 (CH_2), 19.9 (CH_3), 12.7 (CH_3); ESI-MS (+) m/z (z = 2) 395.4 (100), 395.9 (50) [M-2TsO]; (z = 3) 206.7.

2.4 Preparation of liposomal systems

Large unilamellar vesicles have been prepared by hydration of a thin film of POPC, according to the procedure reported in the literature (51). Details are disclosed in Supplementary Materials.

Spectrophotometric measurements were carried out to confirm that guests were embedded into the liposomal bilayer (**Figure 2**).

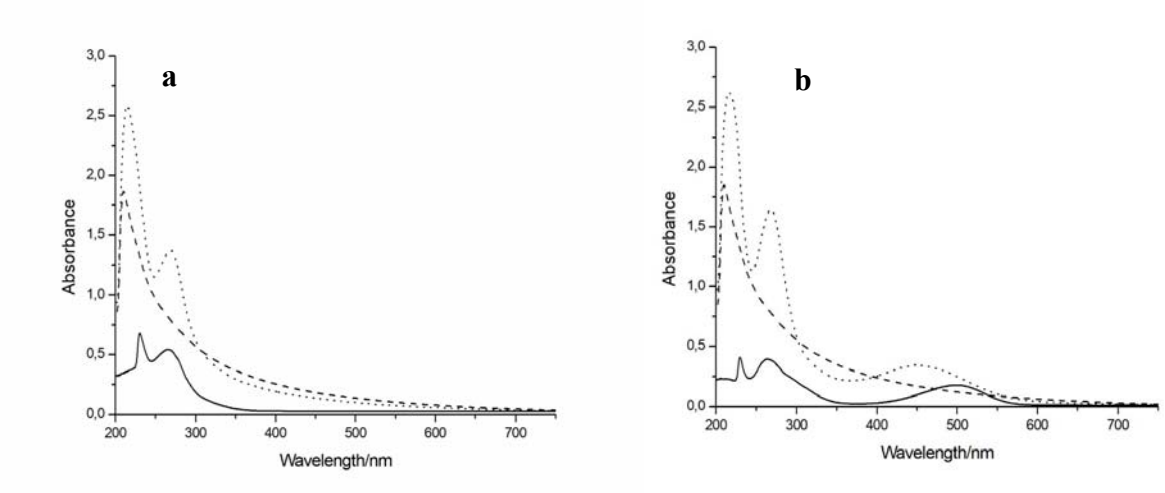

Figure 2. UV/vis spectra of guests **1** and **2** inserted into the liposomes (Figure 1a and 1b, respectively). In Figure 1a, solid line: **1** in CH_2Cl_2; dashed line: pure POPC liposomes in PBS; dotted: **1**/POPC liposomal system in PBS. In Figure 1b, solid line: **2** in CH_2Cl_2/CH_3OH; dashed line: pure POPC liposomes in PBS; dotted line: **2**/POPC liposomal system in PBS.

2.5 Fluorimetric measurements

The microviscosity of the guest-doped liposome bilayer has been determined by using pyrene as the fluorescent probe, according to a well-standardized procedure (52), as reported in Supplementary Materials.

The determination of the stability of liposomes was based on the principle of self-quenching of CF. In fact, while at [CF] = 50 mM the CF fluorescence intensity is low due to its self-quenching, when dilution occurs after the leakage of the entrapped CF from the liposomes, the emission intensity increases due to CF de-quenching. The increase of fluorescence emission intensity at λ = 516 nm, using 490 nm as the excitation wavelength, was followed over a period of 24 h.

For Cl^- transmembrane transport experiments, lucigenin was entrapped in the aqueous core of pure POPC, **1**/POPC, **2**/POPC and **3**/POPC liposomal systems during the hydration step of the phospholipidic films. A Cl^- concentration gradient across the

membrane was created by the addition of NaCl to the liposomal solution. The guest-mediated transport of Cl^- ions into the liposomes was revealed by the quenching of lucigenin fluorescence.

2.6 ^{1}H-NMR titrations

^{1}H-NMR spectra were registered after the addition of increasing amounts of tetrabutylammonium chloride, Bu_4NCl, (range 0.27 – 7.06 mM) to a 2.13 mM solution of tris-(*N*-phenylureido)-calix[6]arene in $CDCl_3$. Similarly, a 5.81 mM solution of calixarene **1** in $CDCl_3$ was titrated with Bu_4NCl (range 1.42 – 18 mM) and spectra were recorded after each Bu_4NCl addition.

2.7 DLS analysis

For size measurements, the autocorrelation function of the scattered light was analyzed assuming a log Gaussian distribution of the vesicle size. The mean size and polydispersity index have been obtained. The ζ potential values were calculated from the electrophoretic mobility by means of the Helmholtz-Smoluchowski relationship.

2.8 Computational section

Two different sets of computational investigations have been carried out. The first one, aimed at understanding the interaction between chloride ion and aromatic moieties (see below) was accomplished by performing Quantum Chemical calculations in the framework of Density Functional Theory (DFT) using the wB97XD functional from Head-Gordon and co-workers (53) which includes empirical dispersion, in conjunction with 6-31+G(d) basis set. Two different minimum energy paths, the first one along the C2v pseudo-symmetry axis of the aromatic ring and the second one orthogonal to the aromatic ring, were scanned. For this purpose, each point was optimized in the presence

of the corresponding symmetry constrain and the character of the interaction energy was analysed through the Molecular Orbital Energy Decomposition Analysis (54) as implemented in the Gamess US program (55). The Basis Set Superposition Error was estimated through the Boys and Bernardi scheme (56). The second set of calculations was aimed at evaluating the work of insertion of axle **3** into POPC bilayer. This was accomplished through MD simulations carried out using the Gromacs package, version 4.5.5 (57) with the Gromos force-field (gromos53a6) (58). The species axle **3** was simulated in the presence a lipid bilayer (POPC). The charges of **3** were calculated using standard fitting procedures with the program Gamess US in the framework of the Density Functional Theory using the same functional and basis set previously referenced. For the lipid bilayer (POPC) we utilized the force field and the equilibrated box taken from the literature (59), and for water, we utilized the Simple Point Charge (spc) model (60). All the simulations were performed in the NVT ensemble with a time step of 2.0 fs adopting a standard protocol: after an initial energy minimization, the system was gradually heated from 50 to 250 K using short (20 ps) MD simulations. Finally, a further pre-equilibration of the system, arrived at 298 K, was carried out by running 1.0 ns of MD simulation in all the systems. The temperature was kept constant using the velocity rescaling procedure (61). The LINCS algorithm was employed to constraint all bond lengths (62). Long-range electrostatic interactions were computed by the Particle Mesh Ewald method with 34 wave vectors in each dimension and a fourth-order cubic interpolation, and a cut-off of 1.1 nm was used (63). All these simulations were aimed at determining the free energy of insertion of **3** within the lipid bilayer adopting the following procedure. First, we performed pulling simulations utilizing a constant velocity steered MD simulation. The center of mass of **3** was pulled in the z-dimension (normal to the bilayer and indicated with ξ in the figures below reported)

forcing **3** to move from the solvent (water) toward the middle of the membrane. A harmonic potential with a force constant of 1000 kJoule mol^{-1} nm^{-2} was adopted in conjunction with constant velocity of 0.001 nm ps^{-1}. Subsequently, starting from the configurations (total number 22 separated by 0.10 nm) generated by the pulling simulations, we carried out Umbrella Sampling (64) in conjunction to the weighted histogram analysis method (WHAM) (65). For this purpose, a harmonic potential of 3000 kJoule mol^{-1} nm^{-2} was applied in the ξ direction between the centre of mass of **3** and the centre of mass of the POPC bilayer. All the 22 simulations were produced and independently produced for 12 ns. The error was evaluated through bootstrap analysis (66). Two further sets of MD simulations of 60 ns were finally carried out with the same protocol: the first one initiated by putting **3**, without any constraint, in the minimum free-energy condition as emerged from the Umbrella Sampling; the second one in the absence of **3**.

3. Results and discussion

3.1 Synthesis of the anion channel components

The calix[6]arene-based anionic channel to be inserted inside the liposomal membrane has been designed based on a known heteroditopic tris-(*N*-phenylureido)calix[6]arene that, as previously shown, is capable to efficiently form "wheel-axle" pseudorotaxane complexes with *N*,*N*-dialkyl viologen-based salts. (67,68) In this work, a new wheel **1** was devised by replacing the phenylureas present onto the calix[6]arene wider rim of the previous systems (24) with the more electron-deficient 4-pyridinureas (see *infra*). Compound **1** was obtained starting from the known triocyloxy-triamino calix[6]arene **4** (see Scheme 1), by converting its amino groups into isocyanates with triphosgene followed by condensation with a molar excess of 4-aminopyridine. The reaction was

carried out in toluene. The characterisation of this new heteroditopic calix[6]arene wheel was carried out through MS and NMR measurements. The ^{1}H NMR spectrum, taken in $CDCl_3$ (see Supplementary Material) show very broad signals, witnessing a large macrocycle fluxionality on the NMR time-scale. HR-MS measurement confirmed the identity of the synthesised compound since the relative m/z spectrum shows peaks relative to the singly, doubly, and triply charged species having isotopes distribution perfectly matching with the theoretic ones (see Supplementary Material). The synthesis of the axial component (**3**) to be transported through the liposomal barrier was challenging. It is a tri cationic two-station thread that in principle can be complexed by **1** through either its 4,4'-bispyridinium group (V-station) or the stilbazolium group (S-station). A long C12 alkyl spacer has been introduced between the two stations. **3** was synthesised in good overall yields through the two-step procedure depicted in Scheme 2. First, the precursor of the S-station, the (*E*)-*N*,*N*-dimethyl-4-(2-(pyridin-4-yl)vinyl)aniline (**5**), was alkylated at its pyridine nitrogen with a large stoichiometric excess (1:7) of dodecane-1,12-diyl ditosylate (**6**) to favour the monofunctionalization of the latter spacer. The excess of **6** is recovered by precipitation from methanol, while the intermediate **7** is reacted as such with the pyridilpyridinium tosylate (**8**) to give the desired thread **3**. Its identity was confirmed as usual by MS and NMR analysis (see Supplementary Material).

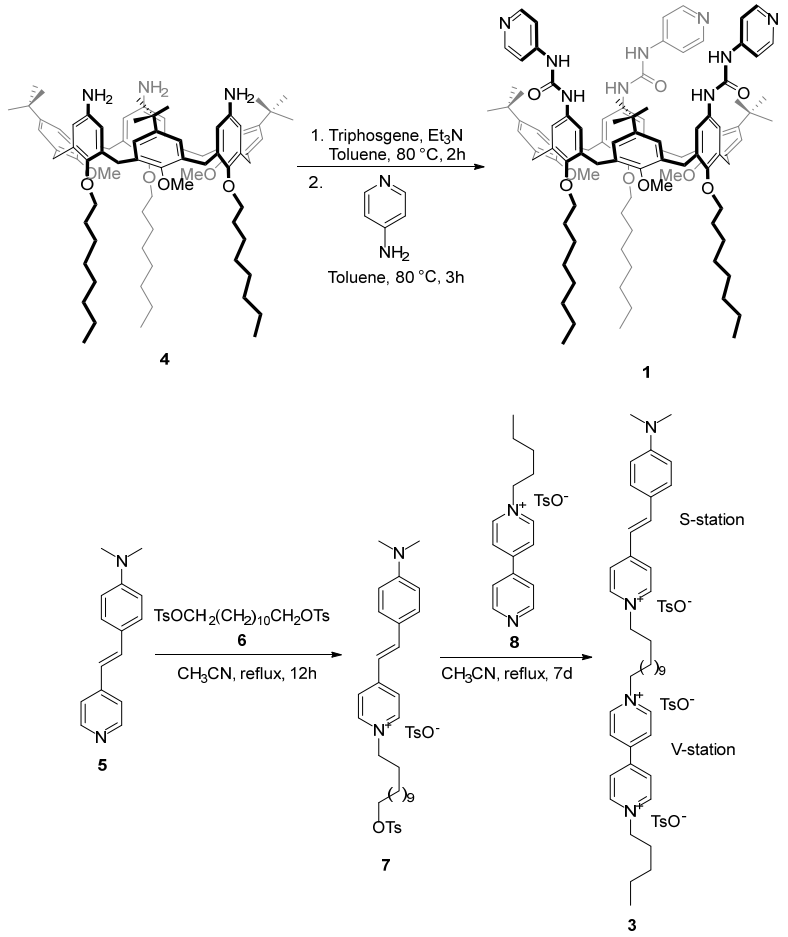

Scheme 2. Synthesis of calix[6]arene wheel **1** and of tricationic axle **3**

Despite its large fluxionality, the ability of **1** to act as a wheel for the viologen salt complexation was verified by NMR with *N*,*N*-dioctyl viologen ditosylate. Upon complexation in $CDCl_3$, indeed, the macrocycle host assumes a pseudo cone conformation characterised by sharper NMR signals (see Supplementary Material). In this geometry the wheel encircles, with its aromatic cavity, the bis-pyridinium unit of the viologen salt and each of the axle two alkyl chains protrudes from the wider and narrow rim of the calix[6]arene (see Scheme 1 or Supplementary Material for a schematic representation of the wheel-axle complexation). As a result, most of the axle resonances result largely upfield-shifted because of the anisotropic shielding effect exerted by the aromatic units of the wheel.

3.2 Characterization of liposomal systems

3.2.1 Determining the microviscosity

The insertion of a guest into a bilayer can alter the bilayer's structural and dynamic characteristics such as mechanical strength, fluidity, and permeation (52, 69, 70). One of the most useful parameters which can be determined to obtain information about the packing and permeability of membranes, is microviscosity (71). The fluorescence spectroscopy, based on the use of environmentally sensitive fluorophores such as pyrene, is the most widely adopted method to determine membrane microviscosity (72-74). Indeed, the emission spectrum of photochemically excited pyrene shows an emission band at 395 nm, due to the pyrene monomer, and an emission band at 480 nm, due to the pyrene excimer whose formation depends on the ability of pyrene to diffuse through the membrane. The parameter C'h, defined by the relation $C'h = (1/k)\eta$, where k is a constant that considers theoretical and instrumental parameters and η is the viscosity, and calculated as the reciprocal of the slope of the straight line obtained by plotting the ratio I_{480}/I_{395} as a function of [pyrene], is used to indirectly express the microviscosity of the liposomal bilayer indirectly. The recorded spectra of pyrene in the liposomal system **1**/POPC (guest/lipid ratio = 2:100), are reported in Figure 3, as an example.

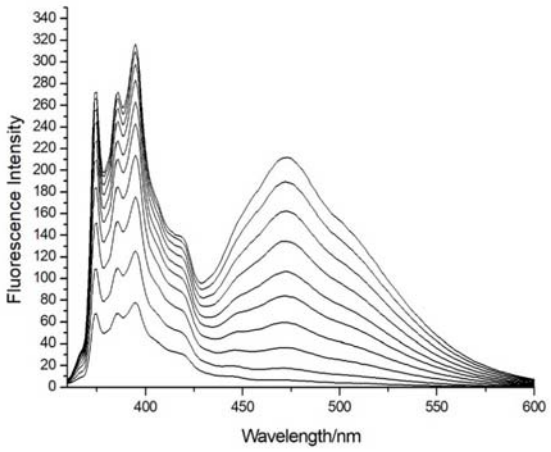

Figure 3. Fluorescent emission spectra of pyrene in the liposomal system **1**/POPC (guest/lipid ratio = 2:100) registered at $1x10^{-6}$ M ≤ [pyrene] ≤ $1x10^{-5}$ M

The data reported in Table 1 show that the insertion in the POPC liposomes of **1** does not alter the membrane microviscosity, suggesting that the molecules of **1** can arrange themselves into the bilayer without affecting the dynamic properties of the membrane thanks to their long hydrophobic tails that match well with the POPC acyl chains. On the contrary, in the presence of both the pseudo-rotaxane **2** and the axle **3**, the microviscosity of the bilayer increases as well as the local polarity experienced by the probe. Indeed, the I_1/I_3 ratio (where I_1 and I_3 correspond to the first and third vibronic bands intensities in the fluorescence spectrum of pyrene, respectively) is very sensitive to the polarity of the environment, and an empirical scale of polarity of pyrene has been introduced by Dong and Winnik (75,76). Presumably, the presence of the hydrophilic axle **3** allows a deeper penetration of water molecules, retained as hydration water. Pyrene molecules which are localized closer to these polar regions, would diffuse more slowly and form less excimers, beeing responsible for the high observed microviscosity.

Liposomal system	C'h (x 10^{-4})	Local polarity
pure POPC	1.59 (± 0.01)	0.978 (± 0.022)
1 + POPC 2:100	1.56 (± 0.01)	0.997 (± 0.011)
2 + POPC 2:100	4.26 (± 0.01)	1.067 (± 0.036)
3 + POPC 2:100	3.49 (± 0.02)	1.046 (± 0.006)

Table 1. C'h parameter and polarity calculated for pure POPC liposomes and guest containing-liposomal systems.

It is worth noting that the results obtained, also rationalized in the light of previous studies present in the literature (see references throughout this section), allowed us to formulate essentially qualitative hypotheses on how guests can interact with bilayer's phospholipids. This interpretation is nevertheless supported by computational analysis (see Section 3.4).

3.2.2 Particle size and zeta potential analysis

Particle size and zeta potential represent valuable sources of information about the physicochemical changes in lipid bilayer upon incorporating a guest (52, 77). Indeed, the insertion of different compounds in the bilayer can promote surface rearrangement inducing alteration of liposomal surface properties but also of the whole lipid bilayer profile, as demonstrated for other ionophores by studies based on ESR technique (47).

The effect of the present guests on the liposome morphology has been investigated by DLS analysis and the liposome surface charge has been quantified by measuring the ζ potential. The obtained results for the three liposomal systems and for pure POPC liposomes are reported in Table 2.

Liposomal system	size (nm) polydispersity index	ζ potential (mV)
pure POPC	118 (± 1) 0.09 (± 0.01)	-20.3 (± 2.1)
1 + POPC 2:100	139 (± 2) 0.13 (± 0.01)	-13.9 (± 1.7)
2 + POPC 2:100	135 (± 8) 0.11 (± 0.02)	-8.49 (± 4.02)
3 + POPC 2:100	113 (± 4) 0.11 (± 0.04)	-2.09 (± 3.71)

Table 2. Liposome size and zeta potential values measured for pure POPC liposomes and for the liposomal systems at guest/lipid ratio = 2:100.

The insertion of **1** and **2**, presumably positioned closer to the lipid-aqueous interface with the long hydrophobic tails pointing toward the liposomal hydrophobic core and the ureido-functionalized rim facing the phospholipid polar heads, leads to a slight increase in the hydrodynamic radius of the liposome. This result is consistent with the liposome enlargement previously observed for the structurally related tris-(N-phenylureido)calix[6]arene (24) explained in terms of different critical packing parameter (CPP). Indeed, each phospholipid type has a characteristic CPP which determines the morphology and the size of the resulting liposomes. The addition of a guest with a CPP higher than that of phospholipids induces the formation of larger aggregates.

The hydrodynamic radius of the **3**/POPC liposomal system does not differ significantly from the value relative to pure POPC liposomes. This is an indication that the axle **3,** due to its hydrophilic character, is not embedded into the bilayer but it presumably resides at the interface between the water and the polar head group.

Regarding the zeta potential values, the insertion of calixarene **1** into POPC liposomes reduces the negative charge on the liposome surface. This result could be due to the ability of the ureido groups of **1** to interact with the phosphate groups of POPC via hydrogen bonding. The H-bonding may reduce the exposure of phosphate head groups and also decrease the head groups mobility inducing the observed change in the surface charge density.

The presence of the positive axle in the pseudo-rotaxane **2** leads to a more marked reduction of the negative charge on the liposome surface. The adsorption of the axle **3** on the liposome surface causes the greatest change in the zeta potential value, due to electrostatic charge neutralization. In this case, the standard deviation indicates a fluctuation of the zeta potential of these liposomal systems that is, in the liposome's population under examination, the net charge of the individual liposomes greatly differs from each other, probably depending on the flexibility of the molecule which may be oriented in different way on the liposomal surface.

3.2.3 Integrity of the liposomal systems

The kinetic stability is a useful parameter to evaluate if a molecule can be properly embedded into a bilayer preserving membrane integrity. Indeed, the incorporation of a guest into the bilayer can alter the physicochemical properties and the structural organization of the membrane, resulting in the formation of pores and defects which allows the efflux of the content of the internal aqueous core into the extra-liposomal environment (78).

The kinetic stability of liposomes can be determined fluorimetrically by monitoring the increase in fluorescence, due to the first order-dequenching of the anionic dye 5(6)-carboxyfluorescein, released from the internal aqueous core of the liposome.

The kinetic profiles of the spontaneous release of CF from pure POPC and from **1**/POPC and **2**/POPC liposomal systems are reported in Figure 4. The values of the calculated first-order rate constants, k_{obs}, for each system are listed in Table 3.

We were not able to carry out the kinetic stability experiments on the liposomal **3**/POPC system as large aggregates are formed in the presence of carboxyfluorescein, which can neither be extruded nor re-solubilized. This is likely due to the electrostatic interaction between the negative probe and the hydrophilic positive axle **3** at the liposome surface.

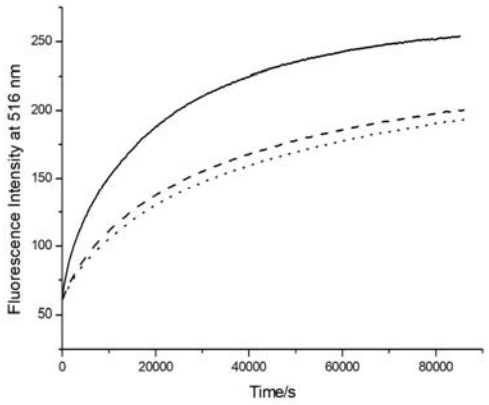

Figure 4. Kinetic profiles of the spontaneous CF release at 25 °C from pure POPC (solid line), **1**/POPC (dotted line) and **2**/POPC (dashed line) liposomal systems.

Liposomal system	k_{obs} x 10^{-4} [s^{-1}]
pure POPC	0.99 (± 0.09)
1 + POPC 2:100	0.56 (± 0.08)
2 + POPC 2:100	0.59 (± 0.03)

Table 3. First order rate constants, k_{obs}, for the spontaneous release of CF from the investigated liposomal systems.

The k_{obs} values reported in Table 3 show that the rate of the release of CF from the internal aqueous core of the liposomes in the extra-liposomal environment is reduced by the insertion of both calix[6] arene **1** and pseudo-rotaxane **2**. Indeed, the stabilizing effect could be due to the favourable hydrophobic interaction between the long alkyl chain of **1** and **2** and the phospholipid tail as well as to hydrogen bonding interaction between the ureido groups of the macrocycles and the phosphate headgroups of POPC. Hydrophobic interactions and hydrogen bonding help to stabilize the membrane hindering the formation of transient pores or defects in the bilayer and lowering the efflux of CF. Similar conclusions were previously reached (24, 79), with hydrogen bonding interactions playing the dominant role in the stabilizing effect of the guests (52).

3.3 Transmembrane transport of chloride ions

The permeability of the membrane-doped liposomes towards chloride ions has been evaluated using lucigenin as the probe to determine the change in Cl^- concentration in the liposomal aqueous core since the fluorescence of lucigenin is quenched upon Cl^- binding. The obtained results are reported in **Table 4**.

Liposomal system	k_{obs} [s^{-1}]
pure POPC	0.0019 (± 0.0001)
1 + POPC 2:100	0.0021 (±0.0001)
2 + POPC 2:100	0.0099 (±0.0001)
3 + POPC 2:100	1.76 (±0.06)

Table 4. First-order rate constants, k_{obs}, for the quenching of lucigenin induced by Cl^- in pure POPC liposomes and in guest-doped liposomes.

Rather in contrast with the experimental evidence available in the literature, for calixarene **1** the predictable anion-π interaction between pyridine ring and chloride ions does not seem to be effective. In fact, the insertion of **1** into the liposomal bilayer does not increase the rate of quenching of lucigenin. This result is even more surprising when compared with the k_{obs} value of 0.0279 (±0.0013) previously obtained for the analogous tris-(*N*-phenylureido)-calix[6]arene (24). Indeed, due to the presence, in calixarene **1**, of the electron-deficient pyridine ring replacing the electron-rich benzene ring in tris-(*N*-phenylureido)-calix[6]arene, we would have expected a higher anion transport activity for calixarene **1**.

The presence of the axle in the **2**/POPC liposomal system favours Cl^- transport across the membrane. This result suggests that the positive charges on the axles in the pseudo-rotaxane can act as anion binding sites, supporting the transport of the anion by electrostatic effect.

Surprisingly, the quenching of lucigenin is very fast for POPC liposomes containing only the axle **3**, as shown by the kinetic profile reported in Figure 5.

The addition of Triton X-100 causes a further decrease in the fluorescence intensity of the lucigenin as the detergent solubilizes liposomes and the remaining lucigenin entrapped is released. Therefore, the effect of Triton X-100 addition to the liposomal suspension gives evidence of the presence of liposomes, also confirmed by DLS analysis, carried out before kinetic measurements, which detects the presence of particles with an average size of 112 (± 4) nm for **3**/POPC 2:100 and 123 (± 1) for **3**/POPC 1:100 liposomal systems.

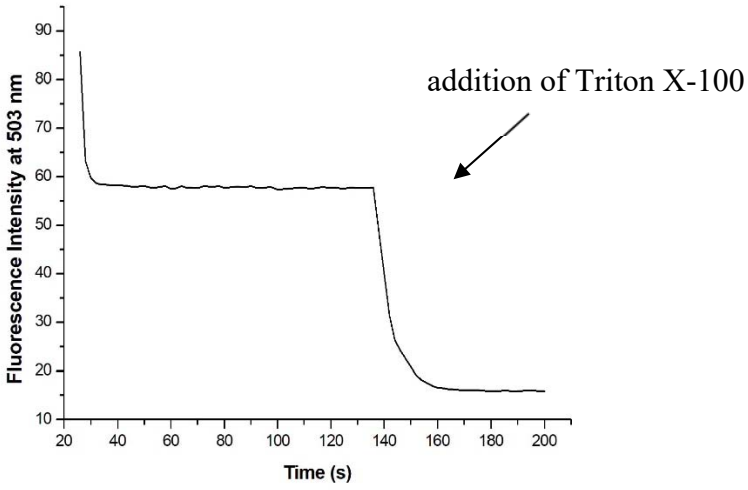

Figure 5. Fluorescence intensity of lucigenin as a function of time after addition of NaCl and after addition of Triton X-100 for **3**/POPC 2:100 liposomal system.

Even if the positively charged axle can bind chloride anions through electrostatic interactions, its hydrophilic character is quite unlikely to allow it to enter the lipophilic bilayer and act as a channel or carrier for chloride ions.

3.4 Computational analysis

To provide a deeper insight for interpreting the obtained results, the interaction energy between chloride ion and aromatic moiety has been evaluated and analyzed through quantum-chemical calculations considering two relative orientations. The first one (see Figure 6a) orthogonal to the plane and hereafter termed as O-orientation, the second one (see Figure 6b) along the C2 pseudo-symmetry axis and hereafter termed as C-orientation. The interaction energy and the corresponding components has been evaluated through the Localized Molecular Orbital Energy Decomposition Analysis (80) based on DFT calculations.

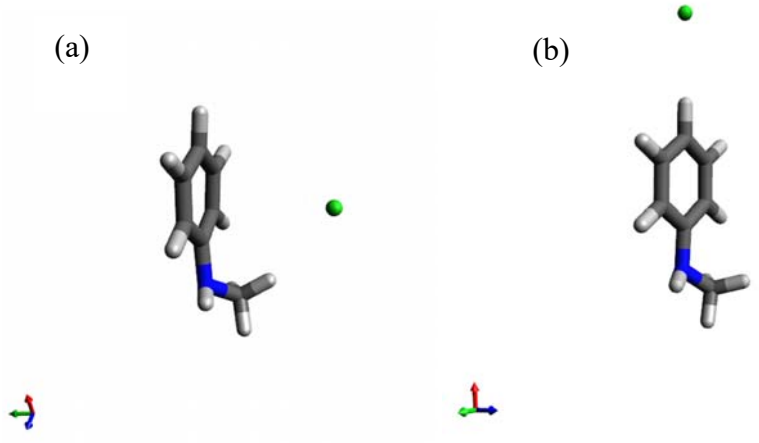

Figure 6. Relative orientations between chloride ion-aromatic ring used in both the systems (phenyl and pyridine): O-orientation (a) and C-orientation (b). For the sake of brevity, we only report the Figures corresponding to the phenyl group.

The profiles of the interaction energy (including the estimation of the basis set superposition error) are reported in Figure 7a for the O-orientation and in Figure 7b for the C-orientation for both systems.

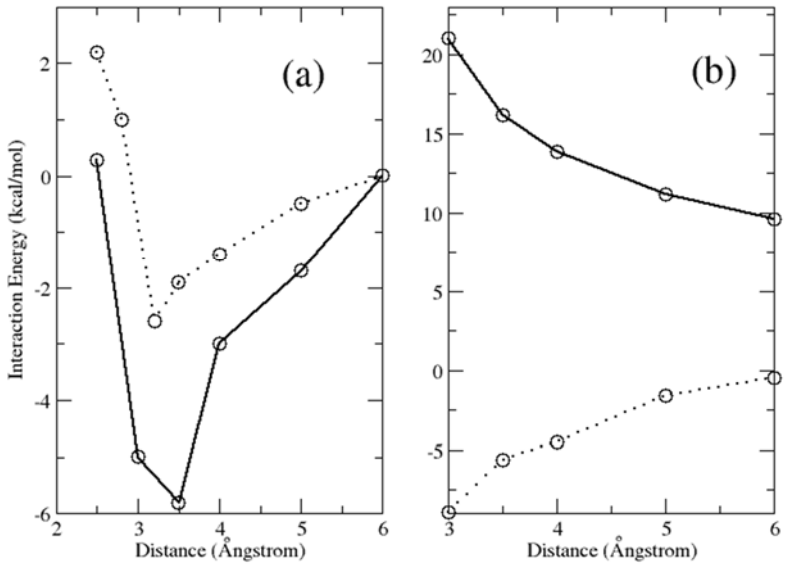

Figure 7. Interaction energy for the O-orientation (a) and for the C-orientation (b). Black line: pyridine; dotted line: phenyl.

When the chloride ion approaches the aromatic ring via C-orientation (Figures 6b and 7b), schematically conceivable as the initial approach to the calixarene, we observe very different behaviours: an attractive interaction for the phenyl ring and a strongly repulsive interaction in the case of pyridine. Such an effect, whose nature is predominantly electrostatic as reported in the Supplementary Material, produces, in the case of the pyridine, a potential energy barrier that somehow slows down or even inhibits the association with the chloride ion. However, once the barrier is overcome, the interaction between chloride and the electron-deficient pyridine moiety (Figures 6a and 7a), which can be perceived as an anion-π interaction, is even more favourable than that between chloride and the phenyl group also due to other effects such as dispersion and exchange (see Supplementary Material) more important at shorter distances. The existence of this potential energy barrier might partially justify the experimental results, which showed a slower transmembrane transfer of chloride ions for **1** compared to tris-(*N*-phenylureido)-calix[6]arene. It is clear that such an analysis should be considered as only indicative because of the possible thermal and solvent effects not considered in the present case.

Moreover, trying to explain the quite surprising results relative to the axle **3**/POPC liposomal system, we modelled the work of insertion of **3** into the liposome. This was accomplished through free-energy calculations based on MD simulations and MD-Umbrella Sampling approach.

For this purpose, we have first estimated the insertion free energy of **3** (at 298 K) as a function of the motion along the direction orthogonal to the bilayer (ξ) surrounded by water, as shown in Figure 8.

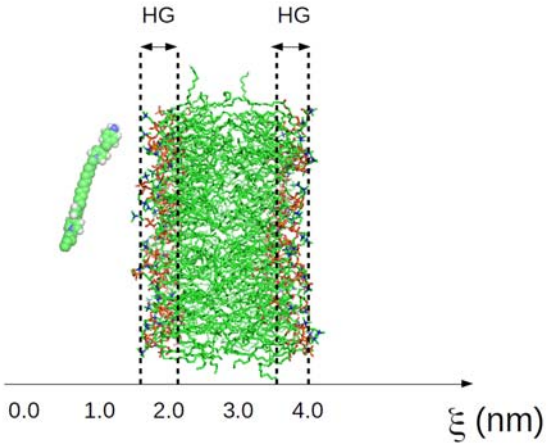

Figure 8. Schematic view of the simulated system (water molecules are omitted for the sake of clarity). In the Figure, we also indicate the water-membrane interface region mainly occupied polar headgroups (HG); for brevity, we hereafter refer to this region as HG region. Note that the abscissa of this Figure (see Figure 8 and also Figure 9), hereafter indicated with ξ, coincides with the direction orthogonal to the bilayer. The zero value of ξ has been arbitrarily taken as the starting point of the Umbrella Sampling procedure.

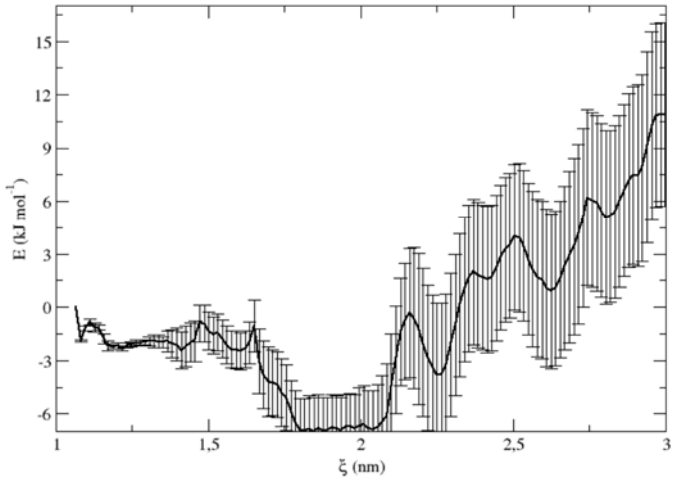

Figure 9. Insertion free energy (and the associated error) as a function of **3** center of the mass. For the definition of the abscissa see the caption of Figure 8.

The resulting profile shown in Figure 9 is characterized by a relatively broad free energy local minimum which, based on the scale of the ξ coordinate explicitly reported in Figure 8, suggests that axle **3** at 298 K is expected to stably reside in the membrane surface, i.e. the region determining the interface between water and the polar head groups. From the same Figure 9 we also note that, according to the free-energy profile, a significant molar ratio of **3** can be found not beyond 2.5 nm along the ξ coordinate, i.e. just below the HG region of Figure 8. Subsequently, we have performed a relatively unbiased long time-scale simulation (60.0 ns) of **3** initially lying on the membrane surface, i.e., within the minimum free-energy basin of the Figure 9. As expected, axle **3** only performs slow oscillations with respect to the surface, as indicated in Figure 10a and it is almost always found in an extended conformation as shown in Figure 10b.

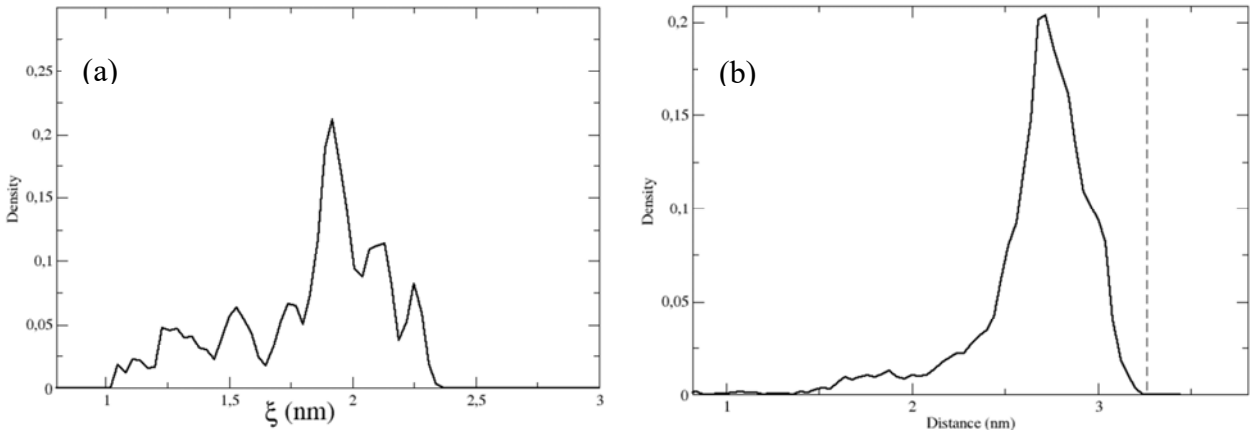

Figure 10. a): distribution of the position of **3** along the x space as found along the unconstrained trajectory. b): distribution of the distance between **3** terminals as found along the trajectory; the dotted line indicates the distance in the fully extended conformation.

From the same unbiased simulation, we also evaluated the possible structural-mechanical effects produced on the membrane by the presence of **3** on the bilayer

surface. For this purpose we have monitored the amount of water molecules present in polar headgroups region of the membrane (indicated as HG in the caption of Figure 8) and compared this result with the one obtained from MD simulation without **3**. The results are reported in Figure 11 where, in the case of MD simulation in the presence of **3**, we have considered the water distribution along the HG region both considering the side facing the approaching **3** (inset c) as well the opposite one (inset b).

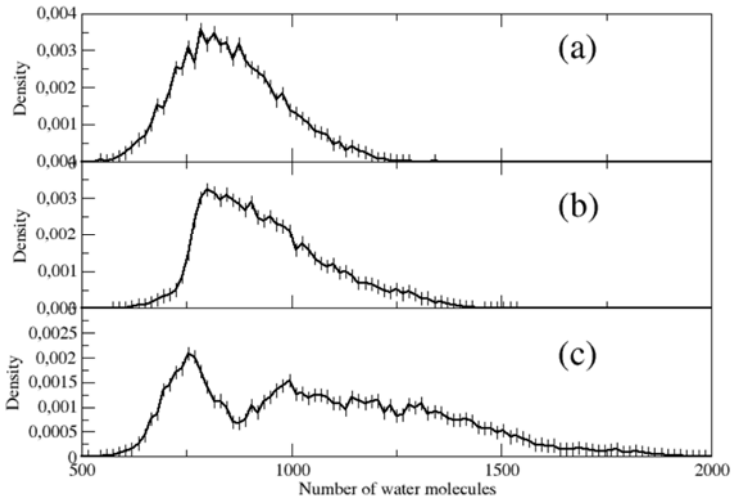

Figure 11. Probability density of water molecules within the HG region. For the free membrane (inset (a)) and the membrane in the presence of **3** both considering the membrane side facing the approaching solute (inset (c)) and the other one. (inset (b)) The error bar has been estimated as a standard error on the average considering three sub-portions of the whole trajectories. Note that in the case of the inset (a) we have reported only one of the two membrane sides as the situation is perfectly superimposable.

From such a Figure it is clear that, within the associated standard error, the presence of **3** on the membrane surface induces a sharp, although not dramatic (which would produce the membrane disruption), increase in water molecules suggesting a clear alteration of the membrane permeability induced by the presence of **3**. Note also that the loss of the symmetry of the distribution in inset (b) is probably the effect of the membrane increased permeation induced by the presence of **3**. For reinforcing such an

observation, we have also carried out a more direct estimation of the membrane mechanical features. In particular, as described more in detail in the Supplementary Material, we have roughly evaluated the possible formation of hydrophilic pores on the bilayer surface. In this respect, in Figure 12, we have reported the size distribution of the surface-pores revealed along the MD simulation both on the side of the membrane directly in contact with **3** (red line) and on the opposite side (black line). As a further confirmation, in the same Figure, we have also reported the result of the same analysis performed on the two sides of the bilayer in the absence of **3**. The rather similar trend of the four distributions clearly indicates that, as expected, the bilayer surface is far from being a rigid structure as the formation of surface-pores is a spontaneous process not necessarily induced by **3**. However, the presence of the latter sharply favors, within the standard error, the formation of medium-sized pores (between 0.5 and 0.9 nm^2) that could be well related to the increase of the permeability of the membrane (Figure 11) not accompanied by its rupture which would presumably be characterized by an increase of the probability of large-sized pores (i.e. increase of the right-tail of the distribution in Figure 12).

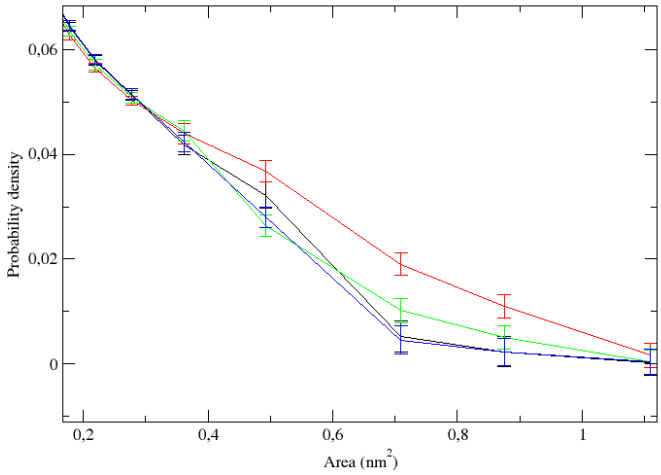

Figure 12. Size distribution of the bilayer surface-holes (see Supplementary Information for additional details) as obtained by monitoring the polar head-groups in the bilayer HG region both in the presence of **3** (the side interacting with **3** is reported in red, the opposite one in black) and in the absence. The error bars are estimations of the standard error obtained by considering three sub-portions of the corresponding MD trajectory.

This evidence is not in disagreement with the very fast quenching of lucigenin experimentally observed for POPC liposomes containing only the axle **3** (Table 4 and Figure 4). Indeed, the presence of **3** on the liposome surface breaks the interactions between phospholipid head groups, allowing the creation of water defects and formation of hydrated hydrophilic pores in the membrane which makes the lipid bilayer permeable to ions. In fact, it has been widely demonstrated that the passage of ions through the membrane can be favoured by the insertion of ionophores that do not act as carriers or channels, but through a non-specific mechanism based on the alteration of the membrane itself, and which does not involve a direct interaction between ion and ionophore. (46,47)

3.5 NMR titration study

^{1}H NMR spectroscopy is a useful method to evidence the occurrence of non-covalent anion-π and hydrogen bonding interactions (40, 41) in solution.

^{1}H NMR spectroscopic titrations with Bu_4NCl were performed in $CDCl_3$ and the recorded spectra are reported in Figure 13 and 14 for tris-(*N*-phenylureido)-calix[6]arene and calixarene **1**, respectively.

Qualitative analysis of the ^{1}H-NMR spectra shows that the addition of Bu_4NCl led to shifted signals for the N-H protons of the ureido groups and aromatic protons for both tris-(*N*-phenylureido)-calix[6]arene and calixarene **1**, suggesting the formation of N-H···Cl hydrogen bonding and also the occurrence of short-contacted interaction of Cl^- ion with aromatic rings of the host molecules.

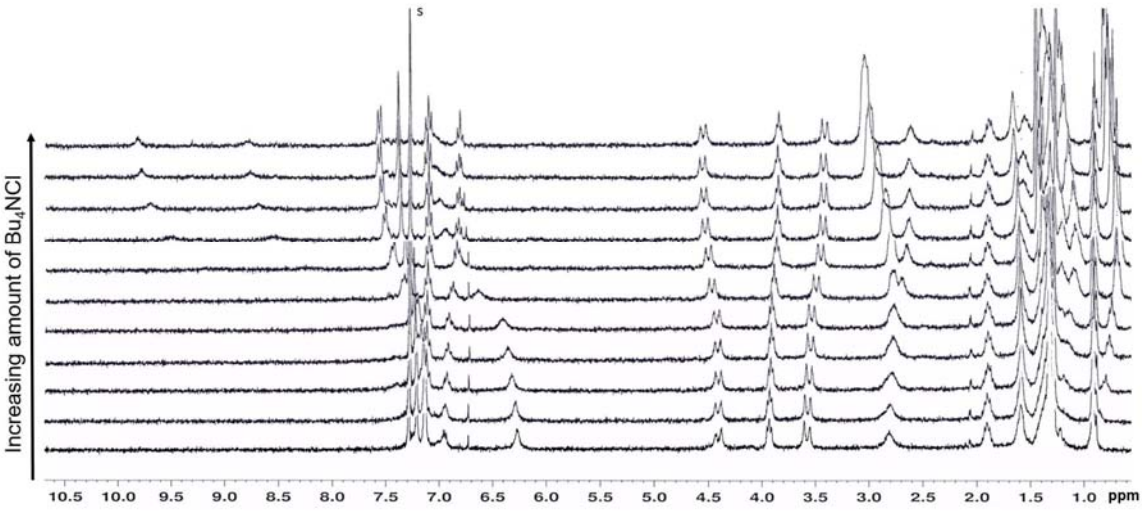

Figure 13. ^{1}H NMR (300 MHz, $CDCl_3$) stack plot showing titration of tris-(N-phenylureido)-calix[6]arene with Bu_4NCl. Chemical shifts of N-H protons change from 6.25 to 7.0 ppm while signals appear at 8.5-8.7 and 9.5-9.8 ppm. Changes in chemical shifts also occur in the range 7.0-7.7 ppm. related to aromatic protons. Final Bu_4NCl /calixarene ratio = 3:1

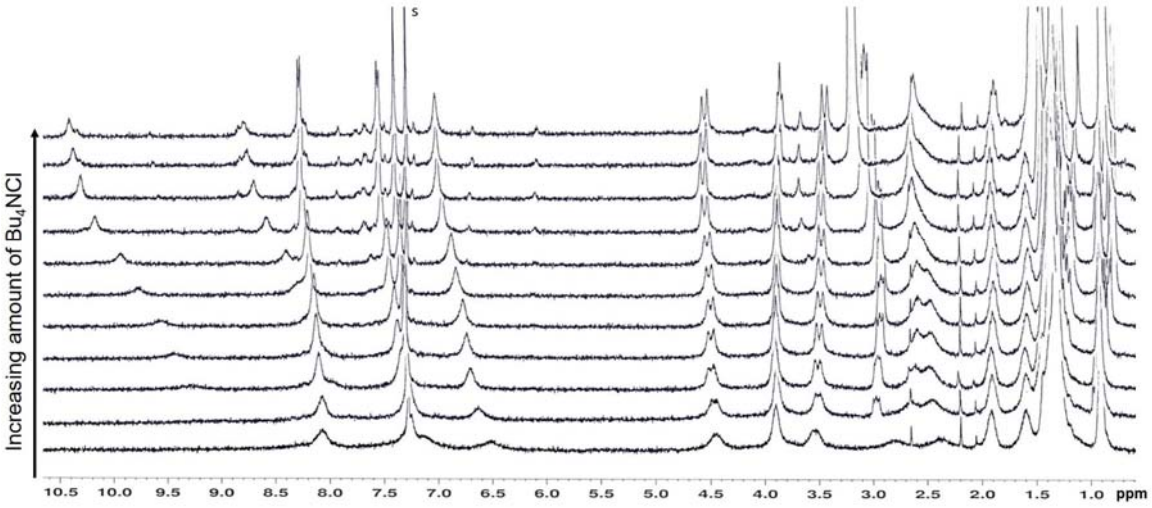

Figure 14. ^{1}H NMR (300 MHz, $CDCl_3$) stack plot showing titration of calixarene **1** with Bu_4NCl. Final Bu_4NCl /calixarene ratio = 3:1.

It is interesting to note that, upon addition of increasing amounts of Cl^-, the very broad signals of **1**, due to a large macrocycle fluxionality on the NMR time-scale, turn into a more distinct peak. In particular, the signals related to the α-protons of the pyridine ring, which are barely visible (7.3 and 8.05 ppm) at $[Cl^-] = 0$, become clearly visible as the Cl^- concentration increases (7.5 and 8.2 ppm at the maximum $[Cl^-]$), suggesting that the interaction of the pyridine moiety with Cl^- ions slows down the dynamic exchange process.

It is noteworthy that, although ^{1}H-NMR spectra reveal that both compounds bind Cl^- ions in organic solution, calixarene **1** cannot transport chloride across the membrane when inserted into lipid bilayers. A tentative explanation of the observed difference could be that, while in solution chloride ion are allowed to come into close contact with the pyridine ring and ureido groups, once embedded into liposomes calixarene organizes itself in a way which does not allow the favourable approach of Cl^- ions via

O-orientation to the pyridine ring. However, due to the interesting evidence here reported, the study is going to be further investigated.

4. Conclusions

The aim of the present study was to analyse the contribution of different non-covalent interactions, i.e. hydrogen bonding, anion-π and electrostatic interactions, in mediating chloride ion transport across phospholipid membrane. Calixarene **1** and the pseudo rotaxane **2** have been suitably designed in order to highlight key structural aspect in modulating Cl^- transport by comparison with the previously studied tris-(*N*-phenylureido)-calix[6]arene. The data obtained support the hypothesis that, once **1** is embedded in the bilayer, a favourable anion-π interaction, which we would have expected from the introduction of the electron-poor ring of pyridine on **1**, can only come into play when a potential energy barrier, due to a repulsive interaction between the pyridine moiety and the chloride ion approaching along the C2 symmetry, is overcome, as quantum- chemical calculations have qualitatively demonstrated.

Indeed, the incorporation of positive charges in the pseudo-rotaxane **2** promotes the transport of chloride ions by electrostatic attraction which, therefore, overcome the initially repulsive electrostatic interaction between Cl^- and pyridine.

Moreover, the presence of positive charges allows the single axle **3** to interact with liposomes at the polar region, resulting in an increase of bilayer permeability originating from an increase of the size of hydrophilic surface-pores which strongly enhance the transmembrane transport of the electrostatically attracted anions.

We believe that our results can provide useful information to define the most appropriate strategy for the rational design and development of optimized anion transporters through appropriate modifications, such as the introduction of positively

charged groups, highly electron-deficient arenes, long hydrophobic tails, which can contribute to ion translocation while preserving membrane integrity.

Notes

There are no conflicts of interest to declare.

Acknowledgements

The authors thank Dr. Silvia Cattani of the Dip.to S.C.V.S.A. of the University of Parma for some NMR and MS measurements. This work was supported by the Italian Ministry of University and Research (PRIN 20173L7W8K KX3) and it has been carried out within the COMP-HUB Initiative, funded by the "Departments of Excellence" program of the Italian Ministry for Education, University and Research (MIUR, 2018–2022). University G. d'Annunzio" supported similarly this work (FAR Fontana-Siani-Di Profio 2018 and 2019). M.A. wishes to thank CINECA (Italy) for an Iscra-C project.

References

(1) D. C. Gadsby, Ion channels versus ion pumps: the principal difference, in principle, Nat. Rev. Mol. Cell Biol. 10, (2009) 344–352, https://doi.org/10.1038/nrm2668 .

(2) F. M. Ashcroft, From molecule to malady, Nature 440, (2006) 440-447, doi: 10.1038/nature04707.

(3) F. M. Ashcroft, Ion Channels and Disease, Academic Press, 2000

(4) J. H. Chen, H. Schulman, P. Gardner, A cAMP-regulated chloride channel in lymphocytes that is affected in cystic fibrosis, Science 243, (1989) 657-660 DOI: 10.1126/science.2464852

(5) P. A. Gale, J. T. Davis, R. Quesada, Anion transport and supramolecular medicinal chemistry, Chem. Soc. Rev. 46, (2017) 2497-2519, DOI: 10.1039/c7cs00159b.

(6) P. H. Schlesinger, R. Ferdani, J. Liu, J. Pajewska, R. Pajewski, M. Saito, H. Shabany, G. W. Gokel, SCMTR: A ChlorideSelective, Membrane-Anchored Peptide Channel That Exhibits Voltage Gating, J. Am. Chem. Soc. 124, (2002,) 1848−1849 https://doi.org/10.1021/ja016784d.

(7) C. Ren, F. Zeng, J. Shen, F. Chen, A. Roy, S. Zhou, H. Ren, H. Zeng, Pore-Forming Monopeptides as Exceptionally Active Anion Channels. J. Am. Chem. Soc. 140, (2018) 8817−8826, https://doi.org/10.1021/jacs.8b04657.

(8) A. Roy, A. Gautam, J. A. Malla, S. Sarkar, A. Mukherjee, P. Talukdar, Self-assembly of small-molecule fumaramides allows transmembrane chloride channel formation. Chem. Commun. 54, (2018) 2024−2027, DOI: 10.1039/c7cc08693h.

9) A. Ikeda, S. Shinkai, Novel cavity design using calix[n]arene skeletons: toward molecular recognition and metal binding, Chem. Rev. 97 (1997) 1713-1734, https://doi.org/10.1021/cr960385x.

(10) O. Danylyuka, K. Suwinska, Solid-state interactions of calixarenes with biorelevant molecules, Chem. Commun. (2009) 5799–5813, DOI: 10.1039/b910331g.

(11) A. Blazejczyk, M. Szczupak, W. Wieczorek, P. Cmoch, G. B. Appetecchi, B. Scrosati, R. Kovarsky, D. Golodnitsky, E. Peled, Anion-Binding Calixarene Receptors: Synthesis, Microstructure, and Effect on Properties of Polyether Electrolytes Chem. Mater. 17 (2005) 1535–1547, https://doi.org/10.1021/cm048679j.

(12) J. Harrowfield, Calixarenes and cations Chem. Commun. 49 (2013) 1578-1580, DOI: 10.1039/c3cc38667h.

(13) G. Arena, A. Contino, F. G. Gulino, A. Magrì, D. Sciotto, R. Ungaro, Complexation of small neutral organic molecules by water soluble calix[4]arenes Tetrahedron Lett. 41 (2000) 9327-9330, https://doi.org/10.1016/S0040-4039(00)01687-7.

(14) Y.-X. Wang, Y.-M- Zhang, Y.-L.- Wang, Y. Liu, Multifunctional Vehicle of Amphiphilic Calix[4]arene Mediated by Liposome Chem Mater. 27 (2015) 2848-2854, https://doi.org/10.1021/cm504653k.

(15) S. Aleandri, A. Casnati, L. Fantuzzi, G. Mancini, G. Rispoli, F. Sansone, Incorporation of a calixarene-based glucose functionalised bolaamphiphile into lipid bilayers for multivalent lectin recognition Org. Biomol. Chem. 11 (2013) 4811-4817, http://doi.org/10.1039/C3OB40732B.

(16) Y. Tanaka, Y. Kobuke, M. Sokabe, A non-peptidic ion channel with K^+ selectivity Angew. Chem. int. Ed. (1995) 34, 693-694, https://doi.org/10.1002/anie.199506931.

(17) N. Yoshino, A. Satake, Y. Kobuke, An artificial ion channel formed by a macrocyclic resorcin[4]arene with amphiphilic cholic acid ether groups Angew. Chem. Int. Ed. (2001) 40, 457-459, https://doi.org/10.1002/1521-3773(20010119)40:2<457::AID-ANIE457>3.0.CO;2-F.

(18) W.H. Chen, M. Nishikawa, S.D. Tan, M. Yamamura, A. Satake, Y. Kobuke Tetracyanoresorcin[4]arene ion channel shows pH dependent conductivity change Chem. Commun. (2004), 872-873, https://doi.org/10.1039/B312952G.

(19) J. de Mendoza, F. Cuevas, P. Prados, E.S. Meadows, G.W. Gokel, A synthetic cation-transporting calix[4]arene derivative active in phospholipid bilayers Angew. Chem. Int. Ed. 37 (1998) 1534-1537, https://doi.org/10.1002/(SICI)1521-3773(19980619)37:11<1534::AID-ANIE1534>3.0.CO;2-B.

(20) I. Izzo, S. Licen, N. Maulucci, G. Autore, S. Marzocco, P. Tecilla, F. De Riccardis, Cationic calix[4]arenes as anion-selective ionophores, Chem. Commun. (2008) 2986-2988, https://doi.org/10.1039/B719482J.

(21) V. Sidorov, F.W. Kotch, G. Abdrakhmanova, R. Mizani, J.C. Fettinger, J.T. Davis, Ion Channel Formation from a Calix[4]arene Amide That Binds HCl J. Am. Chem. Soc. 124 (2002) 2267-2278, https://doi.org/10.1021/ja012338e.

(22) J.L. Seganish, P.V. Santacroce, K.J. Salimian, J.C. Fettinger, P. Zavalij, J.T. Davis, Regulating supramolecular function in membranes: calixarenes that enable or inhibit transmembrane Cl transport. Angew. Chem. Int. Ed. 45 (2006), 3334-3338, https://doi.org/10.1002/anie.200504489.

(23) O.A. Okunola, J.L. Seganish, K.J. Salimian, P.Y. Zavalij, J.T. Davis, Membrane-active calixarenes: toward “gating” transmembrane anion transport, Tetrahedron 63 (2007) 10743-10750, https://doi.org/10.1016/j.tet.2007.06.124.

(24) R. Zappacosta, A. Fontana, A. Credi, A. Arduini, A. Secchi, Incorporation of Calix[6]Arene Macrocycles and (Pseudo)Rotaxanes in Bilayer Membranes: Towards Controllable Artificial Liposomal Channels Asian J. Org. Chem. 4 (2015) 262-270, https://doi.org/10.1002/ajoc.201402244.

(25) P. A. Gale, M. E. Light, B. McNally, K. Navakhun, K. E. Sliwinski, B. D. Smith, Co-transport of H+/Cl– by a Synthetic Prodigiosin Mimic. Chem. Commun. (2005), 3773– 3775, DOI: 10.1039/b503906a.

(26) J. L. Sessler, L. R. Eller, W.-S. Cho, S. Nicolaou, A. Aguilar, J. T. Lee, V. M. Lynch, D. J. Magda, Synthesis, anion-binding properties, and in vitro anticancer activity of prodigiosin analogues. Angew. Chem., Int. Ed. 44 (2005) 5989– 5992, DOI: 10.1002/anie.200501740.

(27) C. C. Tong, R. Quesada, J. L. Sessler, P. A. Gale, Meso-Octamethylcalix[4]pyrrole: an old yet new transmembrane ion-pair transporter. Chem. Commun. (2008), 6321– 6323, DOI: 10.1039/b814988g.

(28) X. Wu, E. N. W. Howe, P. A. Gale, Supramolecular transmembrane anion transport: new assays and insights. Acc. Chem. Res. 51 (2018) 1870– 1879, DOI: 10.1021/acs.accounts.8b00264.

(29) N. Madhavan, E. C. Robert, M. S. Gin, A highly active anion-selective aminocyclodextrin ion channel Angew. Chem., Int. Ed. 44 (2005) 7584– 7587, DOI: 10.1002/anie.200501625.

(30) P.J Costa, I. Marques, V. Felix, Interaction of a calix[4]arene derivative with a DOPC bilayer: biomolecular simulations towards chloride transport, BBA-Biomembranes 1838 (2014), 890-901, https://doi.org/10.1016/j.bbamem.2013.11.021.

(31) J.L. Seganish, J.C. Fettinger, J.T. Davies, Facilitated chloride transport across phosphatidylcholine bilayers by an acyclic calixarene derivative: structure-function relationships, Supramol. Chem. 18 (2006), 257-264, https://doi.org/10.1080/10610270500450010.

(32) V. Gorteau, G. Bollot, J. Mareda, S. Matile, Rigid-rod anion–p slides for multiion hopping across lipid bilayers, Org. Biomol. Chem. 5 (2007), 3000–3012, https://doi.org/10.1039/B708337H.

(33) L. Adriaenssens, C. Estarellas, A. Vargas Jentzsch, M. Martinez Belmonte, S. Matile, P. Ballester, Quantification of nitrate−π interactions and selective transport of nitrate using calix[4]pyrroles with two aromatic walls, J. Am. Chem. Soc. 135 (2013), 8324−8330, https://doi.org/10.1021/ja4021793.

(34) W.-L. Huang, X.-D. Wang, S. Li, R. Zhang, Y.-F. Ao, J. Tang, Q.-Q. Wang, D.-X. Wang, Anion transporters based on noncovalent balance including anion−π, hydrogen, and halogen bonding, J. Org. Chem. 84 (2019) 8859–8869, https://doi.org/10.1021/acs.joc.9b00561.

(35) W.-L. Huang, X.-D. Wang, Y.-F. Ao, Q.-Qi. Wang, D.-X. Wang, Artificial chloride-selective channel: shape and function mimic of the ClC channel selective pore, J. Am. Chem. Soc. 142 (2020) 13273−13277, https://doi.org/10.1021/jacs.0c02881.

(36) M. Mascal, A. Armstrong, M. D. Bartberger, Anion−aromatic bonding: a case for anion recognition by π-acidic rings J. Am. Chem. Soc. 124 (2002) 6274−6276, https://doi.org/10.1021/ja017449s.

(37) I. Alkorta, I. Rozas, J. Elguero, Interaction of anions with perfluoro aromatic compounds J. Am. Chem. Soc. 124 (2002) 8593−8598, https://doi.org/10.1021/ja025693t.

(38) L. M. Salonen, M. Ellermann, F. Diederich, Aromatic rings in chemical and biological recognition: energetics and structures Angew. Chem., Int. Ed. 50 (2011), 4808−4842, https://doi.org/10.1002/anie.201007560.

(39) O. B. Berryman, D. W. Johnson, Experimental evidence for interactions between anions and electron-deficient aromatic rings Chem. Commun., 2009, 3143–3153, DOI: 10.1039/b823236a.

(40) D.-X. Wang, M.-X. Wang, Anion−π interactions: generality, binding strength, and structure" J. Am. Chem. Soc. 135 (2013) 892−897, dx.doi.org/10.1021/ja310834w.

(41) D.-X. Wang, M.-X. Wang, Anion recognition by charge neutral electron-deficient arene receptors" Chimia 65 (2011) 939–943, doi:10.2533/chimia.2011.939.

(42) O. B. Berryman, A. C. Sather, B. P. Hay, J. S. Meisner, D. W. Johnson, Solution phase measurement of both weak σ and C−H···X− hydrogen bonding interactions in synthetic anion receptors J. Am. Chem. Soc. 130 (2008) 10895–10897, DOI: 10.1021/ja8035652.

(43) G. Gil-Ramirez, E. C. Escudero-Adan, J. Benet-Buchholz, P. Ballester, Quantitative evaluation of anion–π interactions in solution Angew. Chem., Int. Ed., 47 (2008) 4114–4118, DOI: 10.1002/anie.200800636.

(44) P. A. Gale, J. T. Davis, R. Quesada, Anion transport and supramolecular medicinal chemistry Chem. Soc. Rev. 46 (2017), 2497—2519, DOI: 10.1039/c7cs00159b.

(45) L. Adriaenssens, C. Estarellas, A. Vargas Jentzsch, M. Martinez Belmonte, S. Matile, P. Ballester, Quantification of nitrate−π interactions and selective transport of nitrate using calix[4]pyrroles with two aromatic walls J. Am. Chem. Soc.135 (2013), 8324−8330, dx.doi.org/10.1021/ja4021793.

(46) E. Busi, G. Vitiello, M. Niccoli, R. Basosi. D. Montesarchio, G. D'Errico, On the mechanism of ion transport through lipid membranes mediated by PEGylated cyclic oligosaccharides (CyPLOS): an ESR study Biochim. Biophys. Acta: Biomembranes 1828 (2013) 2074-2082, https://doi.org/10.1016/j.bbamem.2013.05.017.

(47) G. Vitiello, D. Musumeci, A. Koutsioubas, L. Paduano, D. Montesarchio, G. D'Errico, ionophores at work: exploring the interaction of guanosine-based amphiphiles with phospholipid membranes Biochim. Biophys. Acta: Biomembranes 1859 (2017) 2392-2401, https://doi.org/10.1016/j.bbamem.2017.09.007.

(48) J.J. González, R. Ferdani, E. Albertini, J.M. Blasco, A. Arduini, A. Pochini, P. Prados, J. de Mendoza, Dimeric Capsules by the Self-Assembly of Triureidocalix[6]arenes through Hydrogen Bonds, Chem. Eur. J. 6 (2000) 73–80, https://doi.org/10.1002/(SICI)1521-3765(20000103)6:1<73::AID-CHEM73>3.0.CO;2-%23.

(49) S. Brasselet, F. Cherioux, P. Audebert, J. Zyss, New Octupolar Star-Shaped Strucures for Quadratic Nonlinear Optics, Chem. Mater. 11 (1999) 1915–1920, https://doi.org/10.1021/cm990093n.

(50) A. Boccia, V. Lanzilotto, V. Di Castro, R. Zanoni, L. Pescatori, A. Arduini, A. Secchi, Preparation, reactivity and controlled release of SAMs of calix[4,6]arenes and calix[6]arene-based rotaxanes and pseudorotaxanes formed on polycrystalline Cu, Phys. Chem. Chem. Phys. 13 (2011) 4452–4462, DOI: 10.1039/c0cp01921f.

(51) R. Zappacosta, M. Semeraro, M. Baroncini, S. Silvi, M. Aschi, A. Credi, A. Fontana, Liposome Destabilization by a 2,7-Diazapyrenium Derivative Through Formation of Transient Pores in the Lipid Bilayer Small 6 (2010) 952 –959, https://doi.org/10.1002/smll.200902306.

(52) R. Zappacosta, M. Aschi, A. Ammazzalorso, P. Di Profio, A. Fontana, G. Siani, Embedding calix[4]resorcinarenes in liposomes: Experimental andcomputational investigation of the effect of resorcinarene inclusion on liposome properties and stability BBA - Biomembranes 1861 (2019) 1252–1259, https://doi.org/10.1016/j.bbamem.2019.04.010.

(53) J.-D. Chai, M. Head-Gordon, Systematic optimization of long-range corrected hybrid density functionals *J. Chem. Phys.* 128 (2008) 084106, https://doi.org/10.1063/1.2834918.

(54) P.Su, H.Li, Energy decomposition analysis of covalent bonds and intermolecular interactions J.Chem.Phys. 131 (2009) 014102/1-15, https://doi.org/10.1063/1.3159673

(55) M.W.Schmidt, K.K.Baldridge, J.A.Boatz, S.T.Elbert, M.S.Gordon, J.H.Jensen, S.Koseki, N.Matsunaga, K.A.Nguyen, S.Su, T.L.Windus, M.Dupuis, J.A.Montgomery, General Atomic and Molecular Electronic Structure System J. Comput. Chem. 14, (1993) 1347-1363, https://doi.org/10.1002/jcc.540141112.

(56) S.F. Boys, F. Bernardi, The calculation of small molecular interactions by the differences of separate total energies. Some procedures with reduced errors Molecular Physics 19 (1970) 553-566, https://doi.org/10.1080/00268977000101561.

(57) D. Van der Spoel, E. Lindahl, B. Hess, G. Groenhof, A.E. Mark, H.J.C. Berendsen, GROMACS: fast, flexible, and free J Comput. Chem. 26 (2005) 1701-1718, https://doi.org/10.1002/jcc.20291.

(58) W.F. Van Gunsteren, S.R. Billeter, A.A. Eising, P.H. Hunenberger, P. Kruger, A.E. Mark, W.R.P. Scott, I.G. Tironi Biomolecular Simulation: The GROMOS96 Manual and User Guide Zurich Hochschulverlag AG an der ETH Zurich, Switzerland (1996).

(59) A. Kukol, Lipid models for united-atom molecular dynamics simulations of proteins J Chem. Theo. Comput. 5 (2009) 615-626, https://doi.org/10.1021/ct8003468]

(60) J.C. Berendsen, J.P.M. Postma, W.F. van Gunsteren, J. Hermans, Intermolecular Forces (Ed.), B, Pullman. Reidel, Dordrecht (1981), p. 331.

(61) G. Bussi, D. Donadio, M. Parrinello, Canonical sampling through velocity rescaling J. Chem. Phys. 126 (2007), 014101, https://doi.org/10.1063/1.2408420

(62) B. Hess, H. Bekker, H.J.C. Berendsen, J.C.E.M. Frajie, LINCS: a linear constraint solver for molecular simulations J. Comput. Chem. 18 (1997), 1463-1472, https://doi.org/10.1002/(SICI)1096-987X(199709)18:12<1463::AID-JCC4>3.0.CO;2-H

(63) T.A. Darden, D.M. York, L.G. Pedersen, Particle mesh Ewald: an N·log(N) method for Ewald sums in large systems J. Chem. Phys. 98 (1993), 10089, https://doi.org/10.1063/1.464397.

(64) B. Roux, The calculation of the potential of mean force using computer simulations Comput. Phys. Commun. 91 (1995), 275-282, https://doi.org/10.1016/0010-4655(95)00053-I.

(65) S. Kumar, J.M. Rosenberg, D. Bouzida, R.H. Swendsen, P.A. Kollman THE weighted histogram analysis method for free-energy calculations on biomolecules. I. The method J. Comput. Chem. 13 (1992) 1011-1021, https://doi.org/10.1002/jcc.540130812.

(66) S. Hub, B.L. de Groot, D. van der Spoel, g_wham—A Free Weighted Histogram Analysis Implementation Including Robust Error and Autocorrelation Estimates J. Chem. Theo. and Comput. 6 (2010) 3713–3720, https://doi.org/10.1021/ct100494z.

(67) A. Arduini, G. Orlandini, A. Secchi, A. Credi, S. Silvi, M. Venturi, Calixarene Threading by Viologen-Based Axles, in: P. Neri, J.L. Sessler, M.-X. Wang (Eds.), Calixarenes and Beyond, Springer International Publishing, Cham, 2016: pp. 761–781.

(68) A. Arduini, G. Orlandini, A. Secchi, A. Credi, S. Silvi, M. Venturi, Calix-Based Molecular Machines and Devices, Reference Module in Chemistry, Molecular Sciences and Chemical Engineering. (2014) 1–26.

(69) S. K. Han, J.-S. Kim, Y.-S. Lee , M. Kim, Effect of drug substances on the microviscosity of lipid bilayer of liposomal membrane Arch. Pharm. Res. 13 (1990), 192-197, https://doi.org/10.1007/BF02857799.

(70) A. E. Zhirnov, T. V. Demina, O. O. Krylova, I. D. Grozdova, N. S Melik-Nubarov, Lipid composition determines interaction of liposome membranes with Pluronic L61 Biochim. Biophys. Acta 1720 (2005), 73-83. doi: 10.1016/j.bbamem.2005.11.010.

(71) W. van der Meer, Physiology of membrane fluidity M. Shinitzky (Ed.), CRC Press, Boca Raton, 1984, 1-51.

(72) Y. Barenholz, T. Cohen, E. Haas, M. Ottolenghi, Lateral organization of pyrene-labeled lipids in bilayers as determined from the deviation from equilibrium between pyrene monomers and excimers J. Biol. Chem. 271 (1996) 3085-3090, https://doi.org/10.1074/jbc.271.6.3085.

(73) G. Bains, A.B. Patel, V. Narayanaswami, Pyrene: a probe to study protein conformation and conformational change molecules 16 (2011) 7909-7935, https://doi.org/10.3390/molecules16097909.

(74) N.L. Vekshin, On measuring biomembrane microviscosity using pyrene luminescence in aerobic conditions J. Bioch. Bioph. Methods 15 (1987) 97-104, https://doi.org/10.1016/0165-022X(87)90037-6.

(75) D.C. Dong, M.A. Winnik, The Py scale of solvent polarity. Solvent effects on the vibronic fine structure of pyrene fluorescence and empirical correlations with ET and Y values, Photochem. Photobiol. 35 (1982) 17–21

(76) D.C. Dong, M.A. Winnik, The Py scale of solvent polarities, Can. J. Chem. 62 (1984) 2560–2665

(77) R. Mare, D. Paolino, C. Celia, R. Molinaro, M. Fresta, D. Cosco, Post-insertion parameters of PEG-derivatives in phosphocholine-liposomes Int. J. Phar. 2018, 414-421, https://doi.org/10.1016/j.ijpharm.2018.10.028.

(78) D. Kashchiev, D. Exerova, Bilayer lipid membrane permeation and rupture due to hole formation Biochim. Biophys. Acta: Biomembranes. 732 (1983) 133-145, https://doi.org/10.1016/0005-2736(83)90196-7.

(79) P. De Maria, A. Fontana, C. Gasbarri, D. Velluto, Effects of fullerene guests on the stability of 1-palmitoyl-2-oleoylphosphatidylcholine liposomes Soft Matter 2 (2006) 595-602, http://dx.doi.org/10.1039/B603266D.

(80) P.Su, H.Li, Energy decomposition analysis of covalent bonds and intermolecular interactions J.Chem.Phys. 131 (2009) 014102/1-15, doi.org/10.1063/1.3159673.